NANO · MICRO small
www.small-journal.com

Fabrication of Micropatterned Dipeptide Hydrogels by Acoustic Trapping of Stimulus-Responsive Coacervate Droplets

Madeleine K. Nichols, Ravinash Krishna Kumar, Philip G. Bassindale, Liangfei Tian, Adrian C. Barnes, Bruce W. Drinkwater, Avinash J. Patil, and Stephen Mann**

Acoustic standing waves offer an excellent opportunity to trap and spatially manipulate colloidal objects. This noncontact technique is used for the in situ formation and patterning in aqueous solution of 1D or 2D arrays of pH-responsive coacervate microdroplets comprising poly(diallyldimethylammonium) chloride and the dipeptide *N*-fluorenyl-9-methoxy-carbonyl-D-alanine-D-alanine. Decreasing the pH of the preformed droplet arrays results in dipeptide nanofilament self-assembly and subsequent formation of a micropatterned supramolecular hydrogel that can be removed as a self-supporting monolith. Guest molecules such as molecular dyes, proteins, and oligonucleotides are sequestered specifically within the coacervate droplets during acoustic processing to produce micropatterned hydrogels containing spatially organized functional components. Using this strategy, the site-specific isolation of multiple enzymes to drive a catalytic cascade within the micropatterned hydrogel films is exploited.

Synthesis of hydrogels with unique physical and chemical properties has attracted considerable interest in the field of controlled drug delivery, diagnostics, and tissue engineering.[1] Over the last decade or so, many hydrogel systems based on covalently/noncovalently cross-linked polymers/biopolymers,[2] supramolecular assemblies of amino acid and peptide derivatives,[3–6] and nanocomposite hydrogels encompassing organic–inorganic components have been designed with exceptional mechanical (viscoelastic), chemical (stimuli responsive, self-healing), electrical (conducting), magnetic, and biological properties for desired applications.[7–12] The ability to manipulate hydrogel systems to produce moldable 1D or 2D microscale networks on the microscale is at the center of research fields including tissue engineering and cell biology (cell–matrix interactions, encapsulation, regulation of cell growth, and so on).[13–15] However, the manipulation of hydrogels across these length scales is challenging due to their mechanical characteristics. To date a range of techniques such as soft lithography,[16,17] photolithography,[18,19] laser-guided micropatterning,[20] electromagnetic microfluidics,[21] and 3D printing[22,23] have been implemented to achieve spatial control over hydrogel-based materials.

As an alternative to the above methodologies, acoustic standing waves have recently been employed for the patterning of various microscale objects.[24–30] A typical acoustic device utilizes two or more orthogonally placed piezoelectric transducers (PZTs), which generate waves at the appropriate ultrasonic frequency.[28] Acoustic waves generated in such devices lead to a standing (stationary) pressure field consisting of patterns of nodes (zero pressure) and antinodes (high pressure). A pair of opposed acoustic emitters generates a series of nodal lines, whereas four orthogonally arranged emitters leads to grid-like patterns of nodal points.[31] In both cases, the lines/points are regularly spaced, separated by half of the applied acoustic wavelength. Particles introduced into the standing wave migrate to locations that minimize potential energy, which for relatively dense particles are the pressure nodes where the objects remain immobilized without disturbance.[27] As a result, devices with the ability to generate bulk or surface acoustic waves have been

M. K. Nichols, Dr. R. Krishna Kumar, Dr. L. Tian, Dr. A. J. Patil, Prof. S. Mann
Centre for Organized Matter Chemistry and
Centre for Protolife Research
School of Chemistry
University of Bristol
Bristol BS8 1TS, UK
E-mail: Avinash.patil@bristol.ac.uk; S.mann@bristol.ac.uk
M. K. Nichols, Dr. P. G. Bassindale
Bristol Centre for Functional Nanomaterials
HH Wills Physics Laboratory
Tyndall Avenue, Bristol BS8 1TL, UK
Dr. A. C. Barnes
School of Physics
H H Wills Physics Laboratory
University of Bristol
Bristol BS8 1TL, UK
Prof. B. W. Drinkwater
Department of Mechanical Engineering
University of Bristol
Bristol BS8 1TR, UK
The ORCID identification number(s) for the author(s) of this article can be found under https://doi.org/10.1002/smll.201800739.

DOI: 10.1002/smll.201800739

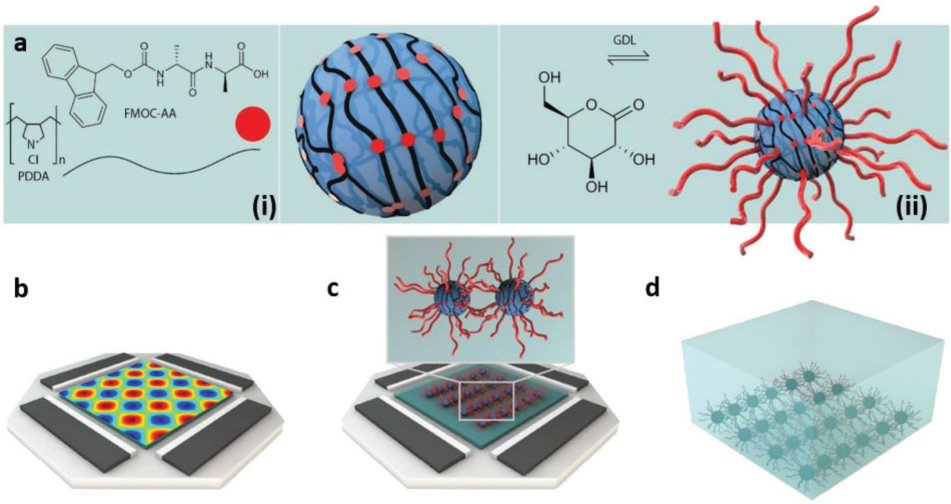

Figure 1. Fabrication of micropatterned dipeptide hydrogels by acoustic trapping of stimulus-responsive coacervate droplets. a) Coacervate components (PDDA, positively charged, black line) and FMOC-AA (negatively charged, red circle) ((i), left), and schematic of coacervate microstructure ((ii), right); equimolar mixing of PDDA and deprotonated FMOC-AA (pH 8) result in electrostatic complexation leading to spontaneous coacervation and formation of spherical microdroplets. (ii) Molecular structure of glucono-δ-lactone (GDL) and schematic illustrating GDL-induced dissociation of the coacervate microdroplets and concomitant dipeptide nanofilament assembly. Slow hydrolysis of GDL lowers the pH from 8 to 4.5, resulting in protonation of the dipeptide. The coacervate droplets act as the initial foci for the transformation process. b) Schematic illustration of the acoustic standing wave trapping device. The trapping device consists of a square central cavity (sample chamber) surrounded by four piezoelectric transducers (white). Additional chambers (black) are filled with water to assist cooling. The transducers are wired in parallel into two pairs such that trapping can be done in 1D or 2D by driving one or both pairs, respectively. Each counterpropagating transducer pair sets up a standing wave acoustic field with stationary zero pressure points or nodes (colored grid-like pattern). c) Acoustic standing wave trapping of pH-responsive polymer-dipeptide coacervate microdroplets (density 1.8 g cm^{-3}) and their transformation into a micropatterned supramolecular hydrogel; PDDA/FMOC-AA coacervate microdroplets are assembled and organized in situ into an ordered grid-like array across the central cavity, spaced by half the wavelength of the applied acoustic wave. After trapping, GDL is introduced into the sample chamber in the presence of the applied acoustic field to produce an array of microdroplets decorated with a corona of dipeptide nanofilaments, which extend outward to produce an entangled network. d) Trapping of the coacervate microdroplets predominantly at the base of the sample chamber leads to spatially organized regions of dense hydrogelation and the formation of periodic stripe patterns in the hydrogel monolith. In contrast, weaker trapping forces along the vertical direction away from the base result in disintegration of the microdroplets in suspension and transformation to a nonpatterned FMOC-AA hydrogel. The partially micropatterned self-supporting hydrogel can be removed from the trapping device.

designed and adapted for spatial manipulation of biomaterials such as cells and bacteria.[32–40] Recently, we demonstrated the application of the acoustic trapping technique for the in situ formation, spontaneous assembly, and spatial organization of polymer–nucleotide coacervates to form microdroplet arrays in aqueous media.[41] The coacervate droplets were prepared by electrostatically mediated liquid–liquid phase separation, and readily sequester a variety of guest species due to the difference in dielectric constant between the external aqueous phase and molecularly crowded interior of the microdroplets.[42] Significantly, the coacervate microdroplets experience an acoustic radiation force in the presence of an acoustic standing wave field because while the difference in compressibility between the droplets and host medium is minimal, the acoustophoretic contrast associated with the difference in density is considerable.[43] As a consequence, gravity-driven sedimentation of the trapped coacervate droplets onto a polyethylene glycol-functionalized substrate produced regular arrays of discrete microdroplets with lattice spacings equal to half of the operating acoustic wavelength. Both 1D and 2D lattices could be generated by using an opposing pair of transducers or four orthogonally arranged emitters, respectively. The studies also demonstrated that enzymes could be spontaneously sequestered into the coacervate phase to produce functional droplet arrays exhibiting spatial and time-dependent fluorescence outputs.

In this study, we use acoustic standing waves to spatially organize a population of stimulus-responsive coacervate microdroplets and exploit these arrays for the in situ construction of micropatterned monoliths of self-assembled hydrogels. To achieve this, square arrays of coacervate microdroplets comprising a cationic polyelectrolyte (poly (diallyldimethylammonium) chloride) (PDDA) and negatively charged dipeptide derivative (*N*-(fluorenyl-9-methoxy-carbonyl)-D-alanine-D-alanine, FMOC-AA) were prepared in the presence of an acoustic standing wave field, and then transformed into a free-standing 1D or 2D micropatterned supramolecular hydrogel in the presence of glucono-δ-lactone (GDL) (**Figure 1**). Transformation of the microdroplet array occurred in situ and was mediated by the slow hydrolysis of GDL which decreased the pH from 8 to 4.5.[44,45] We also show that the selective partitioning of dye molecules, oligonucleotides, and proteins into the PDDA/FMOC-AA coacervate droplets can be exploited to achieve site-specific isolation of the guest molecules within the patterned hydrogel matrix. Using this strategy, we exploit the site-specific isolation of multiple enzymes to drive a catalytic cascade within the micropatterned hydrogel films.

In situ assembly and patterning of pH-responsive polymer–dipeptide coacervate microdroplets was undertaken by using an in-house acoustic trapping device (Experimental Section, and Figure S1, Supporting Information). Simulations of the

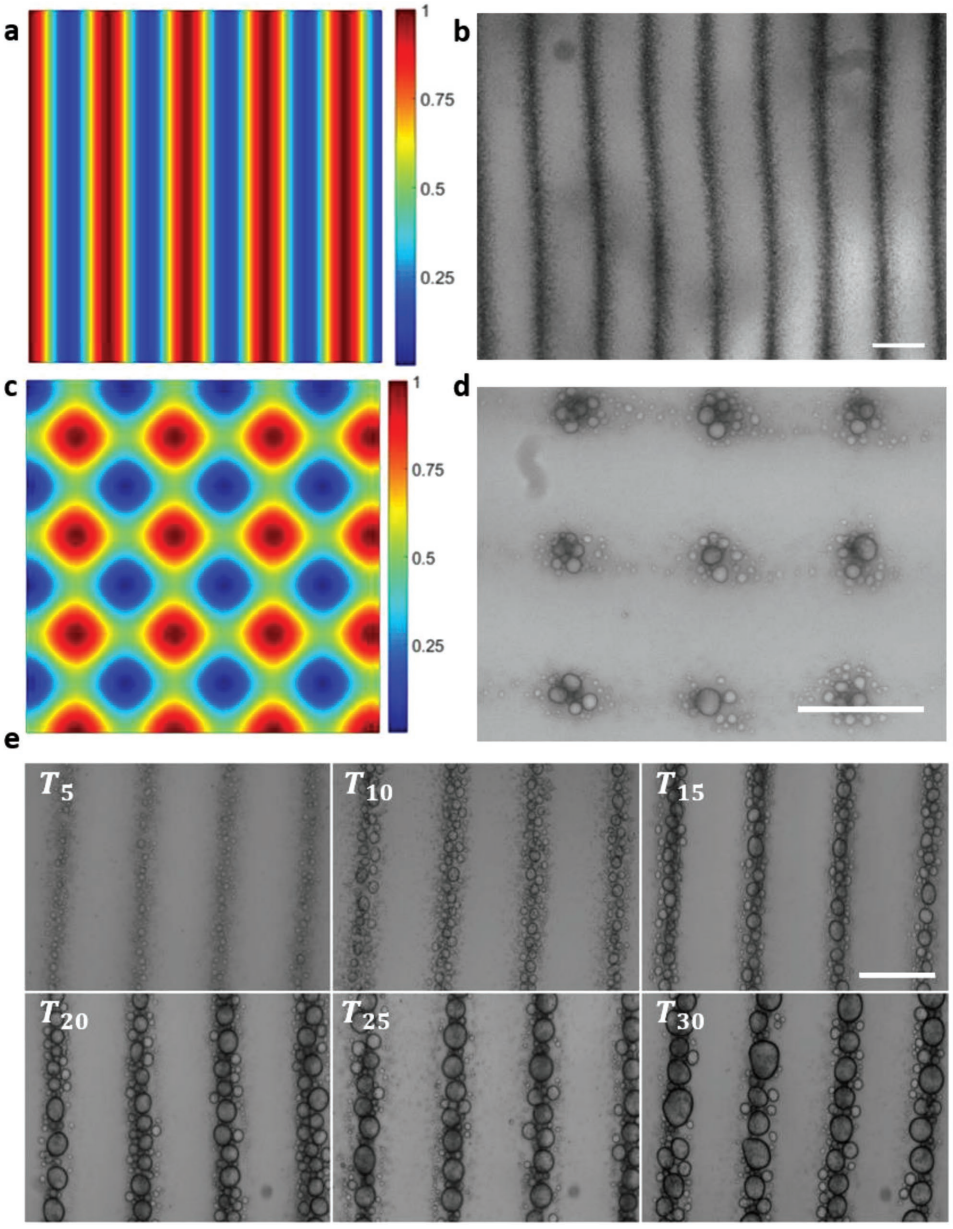

Figure 2. Acoustic standing wave trapping of PDDA/FMOC-AA coacervate microdroplets. a,c) Plane wave simulations of the normalized force fields within the central area of the trapping device, and b,d) corresponding experimental observations. a) 1D simulation generated for an applied acoustic field of 6.7 MHz. Red and blue colored regions show the normalized areas of highest and lowest pressure fields, respectively. b) Corresponding optical microscopy image showing organization of trapped coacervate microdroplets into periodic lines after 5 min. c) 2D simulated pressure field obtained upon activation of four transducers at an operating frequency of 6.7/6.69 MHz with maxima in red and minima in blue. d) Representative optical microscopy image displaying 2D grid-like pattern of regularly spaced coacervate microdroplets located at the nodes. The image is recorded at an early stage in the trapping process (5 min) and shows clusters of small droplets at each nodal point; with time, the small droplets coalesce to produce a single droplet at each node. Samples were prepared at an equimolar ratio of PDDA and FMOC-AA. e) Time-lapse optical microscopy images showing coalescence behavior of PDDA/FMOC-AA (molar ratio 1:1) primary droplets in a 1D acoustic standing wave field (6.7 MHz) over a period of 30 min. Images were acquired every 5 min (denoted as T_x). Discrete spherical droplets are produced within 30 min. Trapping after 30 min results in deformation of the spherical droplets due to contact-induced coalescence with neighboring droplets. Scale bars: 100 μm.

two-transducer and four-transducer acoustic standing wave devices showed periodic arrays of pressure nodes and antinodes in the form of parallel lines and grid-like patterns consistent with 1D and 2D trapping, respectively (**Figure 2**a,c). We used these configurations to produce 1D and 2D spatial patterns of polymer/dipeptide droplets (Figure 2b,d). In both cases, an aqueous PDDA solution (500 μL, 40×10^{-3} M) was added into the central sample chamber of the device under an applied acoustic field, followed by addition of an equimolar aqueous solution of FMOC-AA (500 μL) to produce a turbid suspension of polymer–dipeptide coacervate microdroplets at pH 8. 2D arrays were fabricated using two orthogonally placed pairs of

transducers operated at 6.7/6.69 MHz. The difference in driving frequency (10 kHz) was employed so that the two applied fields were temporally uncorrelated (see the Experimental Section (Simulation Methods)). Time-lapse optical microscopy images showed organized clusters of sub-micrometer sized primary droplets trapped at each nodal point after 5 min of exposure to the acoustic field (Figure 2d). The typical center-to-center spacing was $111 \pm 7 \times 112 \pm 7$ μm, in good agreement with the theoretical half-wavelength spacing (110×110 μm). Prolonged exposure to the acoustic pressure field (30 min) resulted in disruption of the droplets due to increased wetting onto the underlying substrate (Figure S2, Supporting Information).

Coacervate microdroplets were trapped into 1D patterns at the first through-thickness resonant fundamental frequency of the PZT (2.15 MHz) as well as at subsequent harmonics (6.7 and 11.3 MHz) corresponding to half-wavelength pattern spacings of 340, 110, and 63 μm, respectively (Figure S3, Supporting Information). The plane-wave simulations showed that the number of nodal points in the sample cavity (20 mm) were dependent on the frequency used to trap the coacervate microdroplets. Typically, we employed a trapping frequency of 6.7 MHz to produce 1D patterns because the nodal density across the sample cavity gave rise to increased resolution of the antinodal regions under these conditions. Time-lapse optical microscopy images recorded during the formation of the 1D droplet arrays initially showed primary microdroplets of PDDA/FMOC-AA localized around the nodal points of the applied field, followed by the development of ordered line patterns across the entire sample cavity after ≈1 min (Figure S4, Movie S1 (real time), Supporting Information). Subsequent coalescence of the trapped primary droplets produced larger coacervate droplets with a typical diameter of 26 ± 4.4 μm after 30 min (Figure 2e). Increasing charge screening by addition of NaCl in the absence or presence of the applied field disrupted the patterning process and destabilized the coacervate droplets (Figures S5 and S6, Supporting Information).

In light of the above observations, PDDA/FMOC-AA coacervate microdroplets were trapped into 1D or 2D arrays in an acoustic field for 5 min, and then transformed into a self-assembled dipeptide hydrogel by addition of GDL (20×10^{-3} M final concentration) into the sample cavity. Subsequent hydrolysis of GDL to gluconic acid over a period of 12 h in the presence of the acoustic field resulted in a decrease in the pH of the continuous phase from 8 to 4.5 and formation of a FMOC-AA hydrogel monolith that could be removed from the sample chamber as a self-supporting material. The hydrogels were typically $20 \times 20 \times 2$ mm in dimension and exhibited a regular microscale texture that was located specifically towards the side of the hydrogel in contact with the underlying substrate. For example, a 1D acoustic trap operating at 2.15 MHz produced dipeptide hydrogels with distinct regularly spaced 1D lines with a spacing of 355 ± 30 μm (**Figure 3**a), which was commensurate with a predicted value of 340 μm. The line spacing was dependent on the acoustic frequency used to trap the PDDA/FMOC-AA coacervate microdroplets (Figure S7, Supporting Information). Similarly, operating four transducers at acoustic trapping frequencies of 2.15/2.14 MHz produced self-supported hydrogels featuring 2D grid-like patterns that were replicas of the corresponding coacervate microdroplet arrays (Figure 3b). No periodic textures were observed when GDL was added to PDDA/FMOC-AA coacervate microdroplets in the absence of an acoustic field.

As shown in Figure 3a,b, the resolution of the in-plane micropatterned features was highest in areas of the hydrogel associated with the center of the device. To understand this phenomenon, we developed a plane wave model of the lateral plane (*xy*), in which each transducer pair emits 1D plane waves and the total force experienced by the coacervate microdroplets is the sum of the forces generated by the uncorrelated fields in the *xy*-planes (see Simulation Methods). The model predicted that the interference between the uncorrelated orthogonal force fields averages to a negligible value compared to the response time of the coacervate microdroplets to the acoustic field. This gives rise to a highly uniform time-averaged force distribution across the sample chamber (Figure S8a, Supporting Information). However, to account for the effect of the transducer length, the plane wave model was extended using Huygens' principle (Figure S8b, Supporting Information). Significantly, the corresponding simulations revealed highly ordered square grid-like force fields at the center of sample chamber and 1D traps near the transducers or along the walls and corners of the device chamber, which was in good agreement with the patterned features observed in the hydrogel samples.

3D fluorescence confocal image stacks of the 1D micropatterned monoliths revealed that the stripe patterns originated from density differences in the hydrogel network, and extended ≈70 μm in height from the underlying substrate before becoming incoherent (Figure 3c,d). We attributed this to the progressive reduction in the acoustic pressure field along the vertical direction of the sample chamber and disintegration of the nontrapped coacervate microdroplets present in these low-pressure regions into a disordered hydrogel network.[46,44] In contrast, the stripe patterns produced at the base of the hydrogels were attributed to immobilization of the coacervate microdroplets at the acoustic nodal points due to their strong interaction with the surface of the sample cavity. As a consequence, complete dissociation of the trapped coacervate microdroplets was curtailed such that dense hydrogelled cores decorated with a nanofilamentous corona were formed at the acoustic nodes. Subsequent entanglement of the emanating FMOC-AA nanofilaments resulted in a coherent 1D array that was micropatterned into the hydrogel monolith.

Transmission electron microscopy (TEM) image of the acoustically patterned hydrogels confirmed the presence of well-defined FMOC-AA nanofilaments (Figure 3e). Control experiments in which GDL was added to a dispersion of polymer–dipeptide coacervate microdroplets (molar ratio 1:1) showed dipeptide filaments emerging from surface of the droplets, confirming that the droplets act as the initial foci for the transformation process (Figure S9, Supporting Information). Rheological studies on the 1D and 2D patterned hydrogel samples showed frequency sweeps with a linear viscoelastic region where the elastic moduli (G') remained higher than viscous (G'') moduli, consistent with solid-like viscoelastic behavior (Figure 3f). The G' (22×10^3 Pa) and G'' (4×10^3 Pa) values of the 1D hydrogels were similar to those obtained for control samples of unordered FMOC-AA hydrogels prepared

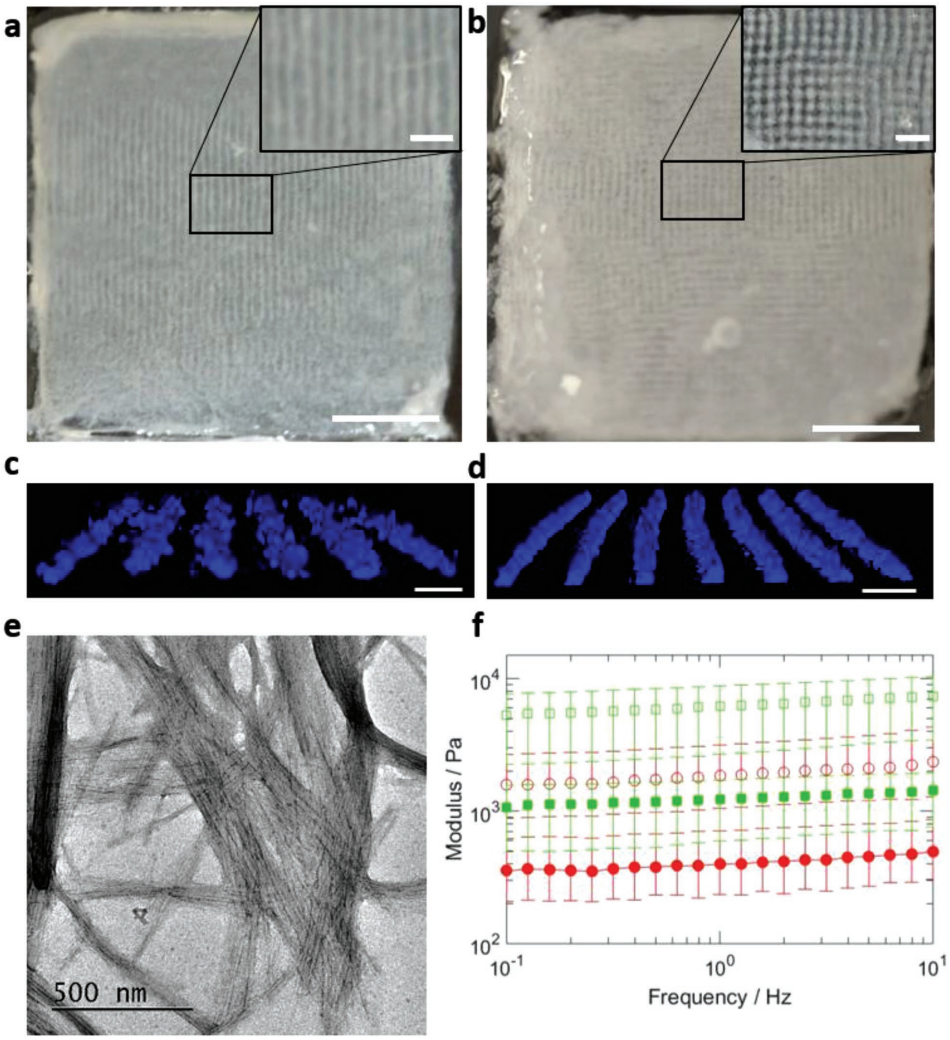

Figure 3. Photographs of acoustically patterned self-supporting dipeptide supramolecular hydrogels. a) 1D patterned hydrogel prepared by GDL-induced in situ transformation of a linear array of PDDA/FMOC-AA coacervate microdroplets in the presence of a 1D acoustic standing wave (2.15 MHz). The periodic line spacing is 340 µm. Inset: magnified region of the hydrogel showing the distinct periodic 1D microtexture. b) 2D patterned dipeptide hydrogel prepared as in (a) but using transducer pairs operating at 2.15/2.14 MHz; inset shows higher resolution detail of the square grid-like arrangement of the hydrogel network. Scale bars: 5 and 1 mm (insets). c,d) 3D confocal fluorescent image stacks of 1D acoustically trapped PDDA/FMOC-AA coacervate microdroplets before and after in situ hydrogelation in an acoustic field (6.7 MHz); samples are stained with Hoechst 33258 dye; scale bars: 120 and 140 µm in (c) and (d), respectively. e) TEM image of uranyl acetate stained nanofilaments generated during pH-induced transformation of an acoustically patterned array of polymer–dipeptide coacervate microdroplets; the FMOC-AA nanofilaments were 12.3 ± 4.3 nm in mean diameter and several micrometers in length. f) Rheology studies showing frequency sweeps obtained for 1D and 2D micropatterned PDDA/FMOC-AA hydrogels. In both cases, storage moduli (G', red (1D) or green (2D) open symbols) and loss moduli (G'', red (1D) or green (2D) color-filled symbols) are consistent with linear (solid-like) viscoelastic behavior ($G' > G''$). Data were averaged in triplicate.

in absence of an acoustic field [G' (25.3×10^3 Pa) and G'' (5×10^3 Pa)] (Figure S10, Supporting Information). In contrast, the 2D patterned hydrogels revealed comparatively lower G' (8.8×10^3 Pa) and G'' (1.7×10^3 Pa) values indicating that the resulting hydrogels were less solid-like (Figure 3f). Oscillatory amplitude sweeps at constant frequency of 1 Hz and strain sweeps of the patterned and nonpatterned control hydrogels exhibited similar deformation properties and extent of their linear viscoelastic regions (Figure S10, Supporting Information).

As control dispersions of the PDDA/FMOC-AA microdroplets prepared in the absence of an acoustic field were capable of sequestering a range of fluorescent dyes, proteins, and ssDNA polymers before and after GDL-induced hydrogelation (Figure S11, Supporting Information), we investigated whether micropatterned FMOC-AA hydrogels with spatially located guest molecules could be fabricated using a combination of acoustic trapping and in situ droplet-to-hydrogel transformation. For this, we used the above procedures to prepare spatially organized lattices of the PDDA/FMOC-AA coacervate droplets but in the presence of fluorescent guest molecules such as the dye Hoechst 33258, FITC-tagged glucose oxidase (FITC-GOx), or a low molecular weight single-stranded CY5-labeled DNA. In each case, confocal fluorescence microscopy images showed that the guest molecules were homogenously partitioned within the acoustically patterned droplet arrays, and that the spatial

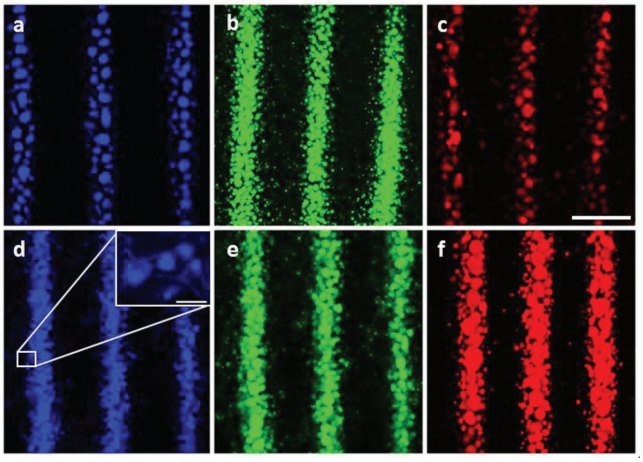

Figure 4. Spatial isolation of guest molecules within 1D acoustically patterned FMOC-AA hydrogels. a–c) Confocal microscopy images showing in situ assembly and trapping of PDDA/FMOC-AA (1:1) coacervate microdroplets with sequestered Hoechst 33258, FITC-GOx, or Cy5-*ss*-DNA. In each case, a homogeneous distribution of the guest molecules is observed, indicating preferential sequestration of the dye, protein, or genetic polymer within the microdroplets. Samples were imaged 5–10 min after addition to the trapping device. d–f) Patterned samples as in (a)–(c) but after GDL-mediated transformation of the trapped coacervate droplets into micropatterned hydrogels. Guest molecules, d) Hoechst 33258, e) FITC-GOx, and f) Cy5-SS-DNA remain preferentially isolated within the dipeptide hydrogel at the loci of the transformed coacervate microdroplets. Hoechst 33258 also binds to the nanofilament network of the dipeptide hydrogel (inset in (d)). No such binding was observed in the presence of FITC-GOx or Cy5-SS-DNA. Scale bar: 100 μm, inset 5 μm

organization of the guest molecules at the nodal lattice points was retained within the hydrogelled cores of the microdroplets after addition of GDL (**Figure 4**). The images revealed the presence of acoustically trapped aster-like structures comprising a core of immobilized fluorescent guest molecules. In contrast, no background fluorescence was observed in the antinode regions.

Using the above strategy, we exploited the site-specific isolation of two enzymes (GOx and horseradish peroxidase (HRP)) to drive a catalytic cascade (**Figure 5**a) within acoustically micropatterned hydrogel films ≈10 μm in thickness. Preformed PDDA/FMOC-AA coacervate microdroplets containing Dylight405-tagged HRP and RITC-tagged GOx were acoustically trapped into a 1D pattern, the supernatant carefully removed, and aqueous GDL injected into the sample chamber in the presence of the acoustic field. Fluorescence optical microscopy imaging confirmed that the droplet arrays were transformed into a 1D micropatterned hydrogel film, and that both enzymes remained encapsulated and spatially organized within the hydrogel cores of the droplet precursors (Figure 5b). Addition of *β*-D-glucose and *o*-phenylenediamine (*o*-PD) to one side of the 1D patterned hydrogel resulted in the onset of green fluorescence specifically within the striped domains of the hydrogel due to conversion of nonfluorescent *o*-PD to fluorescent 2,3-diaminophenazine (2,3-DAP) via the spatially localized GOx/HRP-mediated cascade reaction (Figure 5b). Time-lapse fluorescence microscopy images recorded over a period of 30 min showed a progressive increase in green fluorescence intensity (Figure 5c), indicating that the coupled enzyme reaction could be isolated within the patterned features of the dipeptide hydrogel films. Similar results were obtained for studies undertaken on 2D acoustically micropatterned hydrogels containing GOx and HRP (Figure 5d,e).

In summary, we have demonstrated the application of acoustic standing wave traps for the in situ generation of spatially organized 1D or 2D arrays of stimulus-responsive polymer–dipeptide coacervate microdroplets. In both cases, the pH-induced transformation of the acoustically trapped coacervate microdroplets initiates the supramolecular assembly of FMOC-AA molecules into dipeptide nanofilaments at the surface and core of the PDDA/FMOC-AA microdroplets. Subsequently, entanglement of the nanofilaments in the presence of the acoustic field results in the formation of 1D or 2D micropatterned hydrogels. Critically, the periodic organization of the hydrogelled coacervate microdroplets acts as a template for the formation of 1D or 2D micropatterned features that are retained in the self-supported supramolecular hydrogels. This noncontact patterning technique facilitates the spatial isolation of a range of guest molecules within the hydrogel films such that coupled enzyme reactions can be performed in specific regions of the micropatterned matrix. Our studies suggest that acoustic standing wave-mediated trapping techniques offer a new platform for the construction of micropatterned soft viscoelastic materials relevant to tissue engineering, cell studies, and microarray technologies.

Experimental Section

Acoustic Micropatterning of Dipeptide Hydrogels: In situ coacervate formation and spatial patterning in the presence of an acoustic field was achieved as follows. An aqueous solution of PDDA (40×10^{-3} M) was placed into the central sample cavity of the custom-built acoustic trapping device comprising two oppositely sited transducers operating at frequencies of 2.15, 6.7, or 11.2 MHz and 2.15/2.14, 6.7/6.69, or 11.3/11.29 for 1D or 2D patterning, respectively. An aqueous solution of FMOC-AA (40×10^{-3} M) was then added in the presence of the acoustic field. Formation of polymer–dipeptide coacervate microdroplets in low-pressure areas of the acoustic field occurred typically over a period of 1 min. As a result, patterned 1D or 2D arrays of PDDA/FMOC-AA coacervate microdroplets were produced. To transform the patterned arrays into a patterned hydrogel network, 200 μL of the PDDA/FMOC-AA mixture was removed from the trapping device after formation of the droplet arrays, mixed with a powder of GDL at a final GDL concentration of 20×10^{-3} M, and then carefully replaced back into the trapping device to minimize disruption to the remaining ordered array of coacervate droplets. Any disruption of the pattern was quickly rectified by rapid retrapping of the coacervate microdroplets into 1D or 2D arrays under the applied acoustic field. Samples were then left overnight in a humid environment with the acoustic field applied. During this period, GDL slowly hydrolyzed to reduce the pH to 4.5, thereby initiating the transformation of the droplet array into a micropatterned dipeptide hydrogel. Nonpatterned hydrogels were prepared using the above method but in the absence of the acoustic field.

The above procedures were adapted to prepare acoustically trapped coacervate microdroplets and micropatterned 1D hydrogels containing spatially organized guest molecules. An aqueous mixture of PDDA (40×10^{-3} M) and Hoechst 33258, FITC-GOx, or CY-ssDNA (final concentrations, 6, 6, or 40×10^{-3} M, respectively) was placed in the central sample cavity of the acoustic device in presence of an acoustic standing wave generated by two oppositely placed transducers operating at 6.7 MHz. An aqueous solution of FMOC-AA (40×10^{-3} M) was then

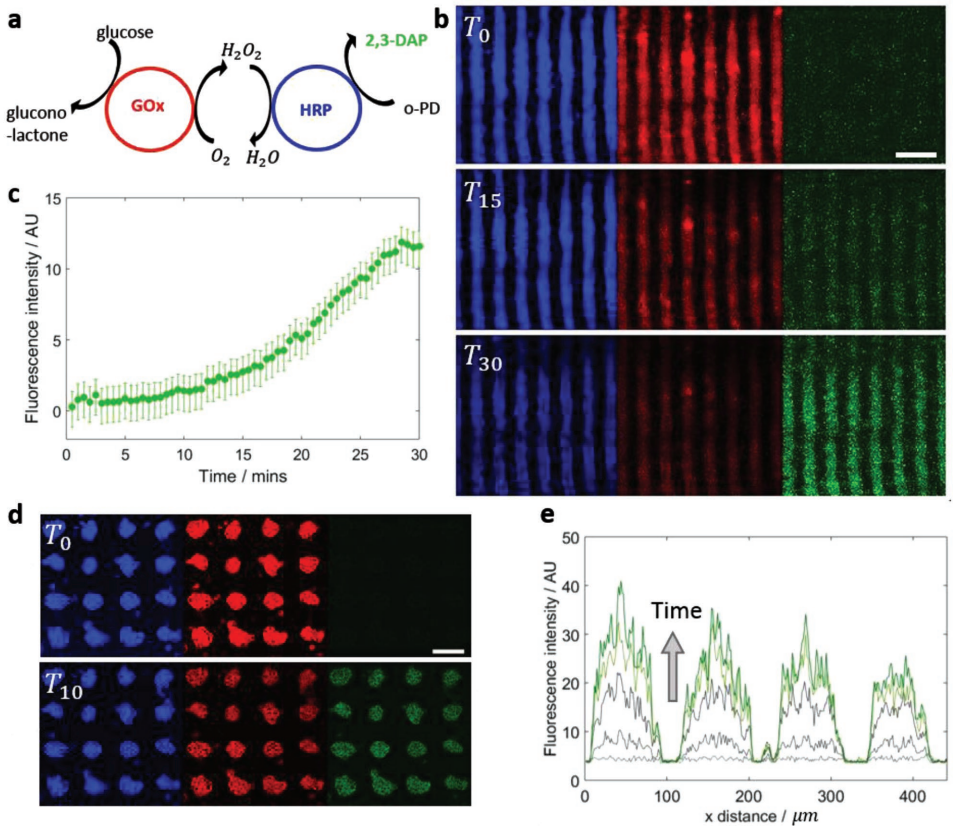

Figure 5. Site-specific catalytic cascade within acoustically micropatterned FMOC-AA hydrogel films. a) Schematic illustration of the GOx/HRP cascade reaction showing conversion of nonfluorescent *o*-phenylenediamine (*o*-PD) to fluorescent 2,3-diaminophenazine (2,3-DAP). b) Time-lapse confocal microscopy images of an enzymatically active 1D micropatterned hydrogel. Images were recorded from three different fluorescence channels every 15 min after the addition of *β*-D-glucose and *o*-PD to the sample chamber. Blue, red, and green fluorescence images show the location of Dylight-405-HRP, RITC-GOx, and 2,3-DAP product, respectively. The enzymes remain immobilized in a periodic stripe pattern throughout the cascade reaction. Production of 2,3-DAP is evidenced by the progressive increase in green fluorescence associated specifically with the enzyme-containing regions of the micropatterned hydrogel. Decreases in red and blue fluorescence intensity with time are due to partial photobleaching. c) Plot of green fluorescence intensity against time showing production of 2,3-DAP in the micropatterned regions of the hydrogel film. Data were extracted from acquired image sets; scale bar, 100 µm. d) Time-lapse confocal microscopy images of an enzymatically active 2D micropatterned hydrogel. Images were recorded from three different fluorescence channels every 10 min after the addition of *β*-D-glucose and *o*-PD to the sample chamber. Blue, red, and green fluorescence images show the location of Dylight-405-HRP, RITC-GOx, and 2,3-DAP, respectively, within the square grid-like array of the patterned hydrogel film. e) Time-dependent green fluorescence intensity measurements recorded across four lattice points showing the spatially organized enzyme-mediated production of 2,3-DAP in the hydrogel. Measurements were taken at 5 min intervals following addition of *o*-PD and glucose to the thin film. Small variations in the maximum peak heights occur due to localized substrate concentration gradients that develop in the hydrogel during the enzyme cascade reaction. Scale bar: 200 µm.

added in the presence of the acoustic field to produce a 1D array of coacervate polymer–dipeptide microdroplets (molar ratio 1:1) containing the sequestered guest molecules. Transformation of the 1D droplet array into a micropatterned hydrogel was achieved as described above.

Enzyme Cascade Reactions in Micropatterned Dipeptide Hydrogel Films: Polymer–dipeptide coacervate microdroplets (PDDA:FMOC-AA = 7:3) containing RITC-tagged glucose oxidase (RITC-GOx) and Dylight-405-tagged horseradish peroxidase (Dylight-HRP) were prepared by addition of both enzymes (20 µL, 1 mg mL^{-1}) to a PDDA solution, followed by addition of FMOC-AA to produce a turbid suspension. Formation of the enzyme-containing coacervate microdroplets was confirmed by optical and fluorescence microscopies (excitations (λ_{ext}) and emission wavelength (λ_{em}) cutoffs: Dylight-405, λ_{ext} = 405 nm, λ_{em} = 410–450 nm; RITC, λ_{ext} = 561 nm, λ_{em} = 570–630 nm). The as-prepared enzyme-containing coacervates were placed in the sample chamber of the acoustic device under a 1D 6.7 MHz standing wave acoustic field. After 1 h, excess supernatant was removed in the presence of the acoustic field by capillary action associated with dipping a paper towel into the corner of the device, and then 1 mL of aqueous GDL (20×10^{-3} M) introduced into the sample chamber. The sample was left overnight under the acoustic standing wave field to initiate hydrogelation of the patterned arrangement of acoustically trapped enzyme-containing coacervate microdroplets. Excess water was subsequently removed from the device with a paper towel to produce a 1D micropatterned hydrogel film comprising immobilized enzymes. Similarly, 2D grid-like patterns of GOx/HRP-containing hydrogel films were fabricated by following the above procedures using an acoustic field generated by four transducers operating in pairs at frequencies of 6.7/6.69 MHz.

A Leica SP5-11 confocal laser scanning microscope was used to follow the enzyme-mediated reactions within the micropatterned hydrogel films. Samples were imaged using a 20× dry lens. To initiate the enzyme cascade reaction within the 1D and 2D micropatterned hydrogel films, an assay mixture containing *β*-D-glucose (20 µL, 300×10^{-3} M, GOx substrate, Sigma Aldrich) and *o*-PD (20 µL, 50×10^{-3} M, HRP substrate, Sigma Aldrich) was added to the thin hydrogel film outside the field of view of the microscope. Diffusion of the substrates into the hydrogel monitored within the field of view resulted in an increase in yellow fluorescence associated with formation of the reaction product 2,3-DAP.

The cascade reaction was monitored by collecting sequential scan images every 30 s with one scan setup used to follow the evolution of the fluorescent product. Sequential scan settings were used for specific filters with the following excitations (λ_{ext}) and emission wavelength (λ_{em}) cutoffs: Dylight-405, λ_{ext} = 405 nm and λ_{em} = 410–450 nm; RITC, λ_{ext} = 561 nm and λ_{em} = 570–630 nm; 2,3-DAP λ_{ext} = 458 nm and λ_{em} = 470–520 nm.

Fabrication of Acoustic Trapping Device: Custom-made acoustic trapping devices were designed using AutoCAD software and the device frame was cut out from polyethylene terephthalate (PET) using a Laser Cutter (Speedy 100 Trotec). PET trapping devices had a central 20 mm square sample cavity, surrounded by four piezoelectric transducers (PZTs) (Noliac, NCE 51, L15 × H2 × W1 mm). The PZT transducers were wired as pairs in parallel. Prior to patterning, a polyethylene glycol (PEG)-functionalized coverslip was adhered to the base of the trapping device, using a flexible adhesive (Fixogum), and the backing wells of the device were filled with water. Electrical impedance measurements on the transducers were undertaken using an Impedance Analyser (Trewmac TE1000 RF). The resonance response of the transducer over frequencies in the range of 1–12 MHz was recorded. Driving frequencies were identified from the minima in the electrical impedance spectra as 2.15, 6.7, and 11.3 MHz. Operating frequencies were applied using a signal generator (Agilent 33220a-001) with a peak-to-peak voltage (V_{pp}) of 10 V. For 2D trapping, a frequency difference of 10 kHz was used between the orthogonal transducer pairs. The trapping frequencies used were 2.15/2.14, 6.7/6.69, and 11.3/11.29 MHz, and each pair were driven by a separate signal generator ensuring that they were temporally uncorrelated.

Characterization: Optical images were acquired using an optical microscope (Leica DMI 3000B). For images of patterned microdroplets, the device was directly mounted onto the microscope. Patterned hydrogels were imaged after removal from the trapping device. Confocal microscopy images were acquired using a Leica SP5-AOBS laser scanning microscope attached to a Leica DMI 6000 inverted epifluorescence microscope. Fluorescent molecules were excited with specific excitation wavelengths and imaged using a 10×/20×/40×/63× objective lens. 3D reconstructions were processed using Volocity cellular imaging and analysis software (V6.3 Visualisation package). Rheological data were obtained using a Malvern Kinexus Pro Rheometer. Small amplitude oscillatory shear (SAOS) measurements were taken using a 20 mm diameter parallel plate geometry for both nonpatterned and patterned hydrogels. All hydrogels were loaded directly onto the rheometer baseplate as self-supporting 20 mm square gels. The test geometry was lowered to a gap height of 1.5 mm and following 10 min of relaxation time, the testing sequence was applied to the sample. 1D patterned hydrogels were loaded with the same orientation of the patterned lines to the baseplate, and nonpatterned hydrogels were prepared in molds with the same size as the sample cavity of the trapping device. All sequences were run at 25° with strain sweeps applied from 0.01–100% at a frequency of 1 Hz, and frequency sweeps from 0.1 to 10 Hz at a strain within the linear viscoelastic region for each hydrogel sample. Each hydrogel was used for only one test and aged for 1 d prior to taking measurements.

Formation of Polymer–Dipeptide coacervates: PDDA (Sigma Aldrich, 100–200 kDa) and FMOC-AA (BAChem) were used as received to prepare 40×10^{-3} M aqueous solutions. Aliquots of 1 M sodium hydroxide were added until a pH of 8.5 was reached to aid dissolution of FMOC-AA in Milli-Q water. The solution was then filtered with a 200 µm filter. Coacervates were prepared by mixing equimolar solutions of 40×10^{-3} M PDDA and FMOC-AA at room temperature and at a final pH of 8, unless otherwise stated.

Sequestration of Guest Molecules in Polymer–Dipeptide Coacervate Microdroplets: Encapsulation of a range of fluorescent guest molecules including Hoechst 33258 (Sigma), fluorescein isothiocyanate (FITC)-tagged glucose oxidase (FITC-GOx, 100 kD, Sigma), and cyanine CY-5 tagged ss-oligoDNA (CY5-ssDNA, 5′-Cy5-ACCACT GAGATCCGGCTGCTAA-3′, Eurofins Genomics) within polymer–dipeptide coacervate microdroplets (molar ratio 1:1) was achieved as follows. In each case, an aqueous solution of the guest molecule at a final concentration of 6×10^{-6} M (Hoechst 33258), 6×10^{-6} M (FITC-GOx), or 40×10^{-6} M (CY5-ssDNA) was added to aqueous PDDA (500 µL, 40×10^{-3} M), followed by addition of aqueous FMOC-AA (500 µL, 40×10^{-3} M), and the resulting droplets imaged using SP5 and SP5II multilaser confocal scanning microscopes with laser excitations at 405 nm (Hoechst 33258), 488 nm (FITC-GOx), and 633 nm (Cy5-ssDNA). Images were acquired with 10× dry or 20×, 40×, and 63× oil immersion lenses. In each case, the fluorescence images showed homogenous sequestration of the guest molecules within the coacervate microdroplets and minimal background fluorescence.

Simulation Methods: Various modeling techniques are available to simulate the acoustic pressure distribution of the acoustic standing wave and resultant acoustic radiation forces on a dispersion of colloidal particles. The simplest such model assumes the transducers to be large and emit plane waves.[31,47] This plane wave assumption leads to the formation of 1D standing waves between each transducer pair, $p(x) = P_0 \cos(kx) \sin(\omega t)$, where P_x is pressure at position x, P_0 is the pressure amplitude, $k = \frac{\omega}{c}$, and ω is the frequency in rad s^{-1}. If a similar 1D standing wave is established in the orthogonal y-axis, then for the case where each pair operates at a different frequency as considered in this paper, the resulting acoustic radiation force on a spherical particle can be written as

$$\boldsymbol{F}(x,y) = F_x \sin(2k_x x)\boldsymbol{e_x} + F_y \sin(2k_y y)\boldsymbol{e_y} \tag{1}$$

where the subscripts denote the direction of the standing waves, symbols in bold are vectors, and e are direction vectors. As can be seen from Equation (1), the x and y force fields act independently and so the total force is the sum of these two contributions. Note that Equation (1) assumes that any interference between these two fields averages to zero over a timescale significantly less than the response time of a particle. This is reasonable as the frequency difference is 10 kHz, implying that 100 cycles of averaging occurs over 10 ms, which is small compared to the time taken for the particles to migrate to the traps (several minutes). The resulting force distribution according to Equation (1) is highly uniform with all traps identical (Figure S6a, Supporting Information).

The plane wave model can be extended to include the effect of finite transducer length (i.e., 15 mm). This is achieved by discretizing the transducers into many line sources, an approach commonly known as Huygens' principle. A discretization level of four-line sources per wavelength was found to lead to convergence of the model. The total pressure for each frequency (i.e., each transducer pair) is then calculated separately. Hence, the acoustic pressure, $P_1(r)$, from a transducer pair operating at ω_1 is given by the summation of the contributions of line sources as

$$P_1(\boldsymbol{r}) = P_0 \sum_{n=1}^{N} \frac{1}{\sqrt{d_n}} e^{i(k_1 d_n)} \tag{2}$$

where P_0 is a constant that scales the amplitude of the pressure field and d_n is the distance from the nth line source to the point, $\boldsymbol{r}$, in the x–y plane. As in the plane wave model, if the transducer pairs operate at different frequencies, then the cross-terms of the total field average to zero. Note in Equation (2) that reflected waves are neglected. However, if required, these can be added to improve the accuracy of the simulation.[48]

The Gor'kov model enables the acoustic radiation force due to an arbitrary pressure field to be predicted.[49] Here, we calculate the total force as the sum of the contributions from transducer pairs operating at different frequencies. As with the plane wave model, we make the reasonable assumption that interference between these two fields averages to zero over a timescale significantly less than the response time of a particle. The force field can then be calculated as

$$\begin{aligned} \boldsymbol{F}(x,y) &= -\nabla\left[U_1(\omega_1) + U_2(\omega_2)\right] \\ U_{1,2}(\omega_{1,2}) &= \frac{4\pi}{3}a^3\left[f_1 \frac{1}{2\rho_0 c_0^2}\left\langle |P_{1,2}|^2 \right\rangle - f_2 \frac{3}{4}\rho_0 \left\langle |v_{1,2}|^2 \right\rangle\right] \\ f_1 &= 1 - \frac{\rho_0 c_0^2}{\rho_p c_p^2} \text{ and } f_2 = \frac{2(\rho_p/\rho_0 - 1)}{2\rho_p/\rho_0 + 1} \end{aligned} \tag{3}$$

where $\langle |P|^2 \rangle$ and $\langle |v|^2 \rangle$ are the mean squared pressure and particle velocity, respectively, at the object, a is the radius of the spherical microparticle being manipulated, ρ is the density, and the subscripts denote the particle, p, or host, 0, properties. For a harmonic sound field, $v = \frac{1}{i\omega\rho_0}\nabla P$. When the transducer size is included in this way, the resulting force field exhibits variations across the central chamber (Figure S6b, Supporting Information). For example, line-like traps are seen near the transducers, whereas point-like traps are seen toward the center of the chamber. This model suggests that transducer size effects are one of the factors that cause the reduced trap uniformity seen when the coacervate microdroplet patterns are observed across the whole chamber. This means that while the local, small-scale (i.e., scales less than a few wavelengths) uniformity is high, there is less consistent patterning on the scale of the chamber.

Supporting Information

Supporting Information is available from the Wiley Online Library or from the author.

Acknowledgements

The authors are grateful for the Bristol Centre for Functional Nanomaterials and EPSRC for funding (Grant No. EP/L016648/1). A.J.P. thanks the University of Bristol, UK, for financial support. L.T. thanks Bris-SynBio for financial support.

Conflict of Interest

The authors declare no conflict of interest.

Keywords

acoustic trapping, coacervates, hydrogels, micropatterning, self-assembly

Received: February 22, 2018
Revised: April 6, 2018
Published online: May 27, 2018

[1] E. A. Appel, J. del Barrio, X. J. Loh, O. A. Scherman, *Chem. Soc. Rev.* **2012**, *41*, 6195.
[2] J. Kopeček, J. Yang, *Angew. Chem., Int. Ed.* **2012**, *51*, 7396.
[3] J. Raeburn, A. Z. Cardoso, D. J. Adams, *Chem. Soc. Rev.* **2013**, *42*, 5143.
[4] D. J. Adams, L. M. Mullen, M. Berta, L. Chen, W. J. Frith, *Soft Matter* **2010**, *6*, 1971.
[5] K. L. Morris, L. Chen, J. Raeburn, O. R. Sellick, P. Cotanda, A. Paul, P. C. Griffiths, S. M. King, R. K. O'Reilly, L. C. Serpell, D. J. Adams, *Nat. Commun.* **2013**, *4*, 1480.
[6] Y. Zhang, H. Gu, Z. Yang, B. Xu, *J. Am. Chem. Soc.* **2003**, *125*, 13680.
[7] A. K. Gaharwar, N. A. Peppas, A. Khademhosseini, *Biotechnol. Bioeng.* **2014**, *111*, 441.
[8] S. Merino, C. Martín, K. Kostarelos, M. Prato, E. Vázquez, *ACS Nano* **2015**, *9*, 4686.
[9] Q. Wang, J. L. Mynar, M. Yoshida, E. Lee, M. Lee, K. Okuro, K. Kinbara, T. Aida, *Nature* **2010**, *463*, 339.
[10] J. E. Martin, A. J. Patil, M. F. Butler, S. Mann, *Adv. Funct. Mater.* **2011**, *21*, 674.
[11] T.-Y. Liu, S.-H. Hu, T.-Y. Liu, D.-M. Liu, S.-Y. Chen, *Langmuir* **2006**, *22*, 5974.
[12] T. Dvir, B. P. Timko, M. D. Brigham, S. R. Naik, S. S. Karajanagi, O. Levy, H. Jin, K. K. Parker, R. Langer, D. S. Kohane, *Nat. Nanotechnol.* **2011**, *6*, 720.
[13] L. G. Griffith, *Science* **2002**, *295*, 1009.
[14] Y. Hu, J. O. You, J. Aizenberg, *ACS Appl. Mater. Interfaces* **2016**, *8*, 21939.
[15] S. Tasoglu, U. A. Gurkan, S. Wang, U. Demirci, *Chem. Soc. Rev.* **2013**, *42*, 5788.
[16] R. S. Kane, S. Takayama, E. Ostuni, D. E. Ingber, G. M. Whitesides, *Biomaterials* **1999**, *20*, 2363.
[17] G. M. Whitesides, E. Ostuni, X. Jiang, D. E. Ingber, *Annu. Rev. Biomed. Eng.* **2001**, *3*, 335.
[18] V. A. Liu, S. N. Bhatia, *Biomed. Microdevices* **2002**, *4*, 257.
[19] Z. J. Wang, C. N. Zhu, W. Hong, Z. L. Wu, Q. Zheng, *Sci. Adv.* **2017**, *3*, e1700348.
[20] M. B. Applegate, J. Coburn, B. P. Partlow, J. E. Moreau, J. P. Mondia, B. Marelli, D. L. Kaplan, F. G. Omenetto, *Proc. Natl. Acad. Sci. USA* **2015**, *112*, 12052.
[21] M.-Y. Chiang, Y.-W. Hsu, H.-Y. Hsieh, S.-Y. Chen, S.-K. Fan, *Sci. Adv.* **2016**, *2*, e1600964.
[22] A. A. Pawar, G. Saada, I. Cooperstein, L. Larush, A. J. Jackman, S. R. Tabaei, N.-J. Cho, S. Magdassi, *Sci. Adv.* **2016**, *2*, e1501381.
[23] Z. Wu, X. Su, Y. Xu, B. Kong, W. Sun, S. Mi, *Sci. Rep.* **2016**, *6*, 24474.
[24] R. R. Collino, T. R. Ray, R. C. Fleming, C. H. Sasaki, H. Haj-Hariri, M. R. Begley, *Extreme Mech. Lett.* **2015**, *5*, 37.
[25] T. M. Llewellyn-Jones, B. W. Drinkwater, R. S. Trask, *Smart. Mater. Struct.* **2016**, *25*, 02LT01.
[26] Y. Chen, X. Ding, S. C. S. Lin, S. Yang, P. H. Huang, N. Nama, Y. Zhao, A. A. Nawaz, F. Guo, W. Wang, Y. Gu, T. E. Mallouk, T. J. Huang, *ACS Nano* **2013**, *7*, 3306.
[27] P. Glynne-Jones, R. J. Boltryk, M. Hill, *Lab Chip* **2012**, *12*, 1417.
[28] C. R. P. Courtney, C. K. Ong, B. W. Drinkwater, A. L. Bernassau, P. D. Wilcox, D. R. S. Cumming, *Proc. R. Soc. A* **2012**, *468*, 337.
[29] M. Evander, J. Nilsson, *Lab Chip* **2012**, *12*, 4667.
[30] C. E. Owens, C. W. Shields, D. F. Cruz, P. Charbonneau, G. P. López, *Soft Matter* **2016**, *12*, 717.
[31] B. W. Drinkwater, *Lab Chip* **2016**, *16*, 2360.
[32] A. Haake, J. Dual, *Ultrasonics* **2004**, *42*, 75.
[33] Y. Ai, C. K. Sanders, B. L. Marrone, *Anal. Chem.* **2013**, *85*, 9126.
[34] S. C. Takatori, R. De Dier, J. Vermant, J. F. Brady, *Nat. Commun.* **2016**, *7*, 10694.
[35] B. Hammarström, B. Nilson, T. Laurell, J. Nilsson, S. Ekström, *Anal. Chem.* **2014**, *86*, 10560.
[36] A. L. Bernassau, F. Gesellchen, P. G. A. MacPherson, M. Riehle, D. R. S. Cumming, *Biomed. Microdevices* **2012**, *14*, 559.
[37] X. Ding, S.-C. S. Lin, B. Kiraly, H. Yue, S. Li, I.-K. Chiang, J. Shi, S. J. Benkovic, T. J. Huang, *Proc. Natl. Acad. Sci. USA* **2012**, *109*, 11105.
[38] F. Guo, P. Li, J. B. French, Z. Mao, H. Zhao, S. Li, N. Nama, J. R. Fick, S. J. Benkovic, T. J. Huang, *Proc. Natl. Acad. Sci. USA* **2015**, *112*, 43.
[39] P. Li, Z. Mao, Z. Peng, L. Zhou, Y. Chen, P.-H. Huang, C. I. Truica, J. J. Drabick, W. S. El-Deiry, M. Dao, S. Suresh, T. J. Huang, *Proc. Natl. Acad. Sci. USA* **2015**, *112*, 4970.
[40] D. J. Collins, B. Morahan, J. Garcia-Bustos, C. Doerig, M. Plebanski, A. Nield, *Nat. Commun.* **2015**, *6*, 8686.
[41] L. Tian, N. Martin, P. G. Bassindale, A. J. Patil, M. Li, A. Barnes, B. W. Drinkwater, S. Mann, *Nat. Commun.* **2016**, *7*, 13068.

[42] D. S. Williams, S. Koga, C. R. C. Hak, A. Majrekar, A. J. Patil, A. W. Perriman, S. Mann, *Soft Matter* **2012**, *8*, 6004.
[43] J. T. Karlsen, P. Augustsson, H. Bruus, *Phys. Rev. Lett.* **2016**, *11*, 114504.
[44] R. K. Kumar, R. L. Harniman, A. J. Patil, S. Mann, *Chem. Sci.* **2016**, *7*, 5879.
[45] D. J. Adams, M. F. Butler, W. J. Frith, M. Kirkland, L. Mullen, P. Sanderson, *Soft Matter* **2009**, *5*, 1856.
[46] M.-S. Scholz, B. W. Drinkwater, T. M. Llewellyn-Jones, R. S. Trask, *IEEE Trans. Ultrason. Ferroelectr. Freq. Control* **2015**, *62*, 1845.
[47] F. Guo, Z. Mao, Y. Chen, Z. Xie, J. P. Lata, P. Li, L. Ren, J. Liu, J. Yang, M. Dao, S. Suresh, T. J. Huang, *Proc. Natl. Acad. Sci. USA* **2016**, *113*, 1522.
[48] M. A. B. Andrade, N. Pérez, F. Buiochi, J. C. Adamowski, *IEEE Trans. Ultrason. Ferroelectr. Freq. Control* **2011**, *58*, 1674.
[49] L. P. Gorkov, *Dokl. S I Vavilov Inst. Phys. Probl.* **1962**, *6*, 773.